Int. J. Environ. Sci. Technol. (2014) 11:571–588
DOI 10.1007/s13762-013-0256-6

ORIGINAL PAPER

A wastewater treatment using a biofilm airlift suspension reactor with biomass attached to supports: a numerical model

P. Viotti · A. Luciano · G. Mancini · V. Torretta

Received: 15 April 2012 / Revised: 12 February 2013 / Accepted: 9 March 2013 / Published online: 18 April 2013

Abstract A mathematical model of the biological process occurring in a modified biofilm airlift suspension reactor is presented. When compared with a traditional wastewater treatment plant, a biofilm airlift suspension process has major advantages, such as higher oxygen levels in the bulk fluid and lower space requirements. The limited volumes obtained with this technique generally do not allow to reach the high times of contact required for an efficient removal of nitrogen that normally are characterized by a slower kinetics than carbonaceous compounds. To avoid this problem, supports for attached biomass growth were inserted in the reactor. Both physical and biological aspects were incorporated into the presented model to simulate the removal processes of the substrates. A sensitivity analysis was performed, and the model was validated using experimental results obtained at a lab-scale plant. This model can accurately estimate the removal rate in different boundary conditions providing the details of the water quality profiles through the reactor and in the attached biomass. The model thus represents a valid aid for design purposes and for the management of treatment plants that use these uncommon reactors. The model also provides the required hydraulic retention time for a complete nitrification and the appropriate recirculation ratio. The results have shown the full-scale applicability of this treatment due to its efficiencies coupled to the advantages of its low impact, low space requirement and low sludge production.

Keywords Modified biofilm airlift suspension reactor · Attached biomass · Flux model · Biofilm model · Sensitivity analysis · Simultaneous nitrification–denitrification

P. Viotti
Department of Civil, Building and Environmental Engineering (DICEA), Sapienza University of Rome, Via Eudossiana 18, 00184 Rome, Italy

A. Luciano (✉)
ENEA, Italian National Agency for New Technologies, Energy and Sustainable Economic Development - RC Casaccia, Via Anguillarese 301, 00123 Rome, Italy
e-mail: antonella.luciano@enea.it

G. Mancini
Department of Industrial and Mechanical Engineering, University of Catania, Via A Doria 6, 95125 Catania, Italy

V. Torretta
Department of Science and High Technology, Insubria University of Varese, Via G.B. Vico 46, 21100 Varese, Italy

Introduction

Biofilm reactors can be applied in conditions, where the reactor efficiency, obtained using only freely suspended organisms, is limited by the biomass concentration and by short hydraulic residence time. Cases can be encountered either for slow-growing organisms (e.g., nitrifiers and de-nitrifiers), whose growth in suspension requires long residence times, or diluted feed streams (a situation frequently found in domestic wastewater treatment processes), in which only very low biomass concentrations can be achieved without biomass retention (Nicolella et al. 2000; De Feo 2007). In these cases, biofilms can represent an effective solution to successfully retain biomass in the reactors and to improve the volumetric conversion capacity (Nicolella et al. 1998; Splendiani et al. 2006). Several technologies at low space requirement based on the biofilms have been developed as alternatives to the traditional wastewater treatment (Nicolella et al. 2000; Akhbari et al.

2012). In recent years, many of these technologies have been tested and applied, mainly for the industrial wastewater, to pilot and full-scale plants. The importance of developing new technologies also in the civil field is linked to the high space requirements of conventional treatment plants (mainly activated sludge systems) and to the related high impacts on populations in terms of noise and odours production (Walter et al. 2005). Airlift technology reactors represent a potential solution, where the high oxygen levels in the stream assure both high efficiencies and low odour impact. However, the design and management of these less common treatment plants can require a numerical tool able to analyze and control the different processes involved. At the beginning of the 1970s, several mathematical models were developed to link the substrate flux into the biofilm to the fundamental mechanisms of substrate utilisation and mass transport (Harremoës 1976; La Motta and Mulcahy 1978; Williamson and Mc Carty 1976; Rittmann and McCarty 1980). The main goal (aim) of these first-generation mechanistic models was to describe the mass flux into the biofilm and the concentration profile of one rate-limiting substrate within the biofilm (Wanner et al. 2006). Later, the biofilm models evolved from one-dimensional spatial models to multidimensional models, from single species models to multispecies models, from steady-state models (Mudliar et al. 2008) to dynamical models (Russo et al. 2008), and from pure growth models to models involving biomass growth (Jiang et al. 2009; Rahman et al. 2009) and biofilm–fluid interactions, etc. (Wang and Zhang 2010). Empirical models for the evaluation of the overall reactor performance have been reconsidered in recent years (Wang et al. 2006; Piciorenau et al. 2004). Biofilms are complex systems, therefore, a biofilm model that attempts to consider all the complexities should include: (i) mass balance equations for all of the processes occurring, for all components, in all compartments, (ii) continuity and momentum equations for the fluid in all compartments, and (iii) defined conditions for all variables at all system boundaries. However, even the most complex biofilm models existing today contain many simplifying assumptions, because of the difficulties in applying this approach to all the system components. Actually, a model should be as simple as possible, and only as complex as needed (Wanner et al. 2006); especially, when it is not used to verify theoretical or experimental findings, but to make qualitative and quantitative predictions that might well serve as guidelines for several aspects of design (Wang and Zhang 2010). If the objective is then to describe the performance at the macro-scale, a detailed analysis at the micro-scale could be redundant (Wanner et al. 2006; Morgenroth et al. 2004). The use of a simple model for engineering purposes is also fundamental in the design of technologies that cannot be represented through a simple completely mixed reactor approach. This could significantly enhance the use of numerical models for the design of more efficient or innovative domestic sewages treatments (Noguera et al. 1999). The reactor here presented is designed on the basis of the traditional deep shaft technology, but the addition of fixed supports for the attached biomass growth is also considered to achieve higher removal efficiency. The main objective of this work is to provide a tool for the design and management, on a full scale, of the combination of the two technologies (i.e., biofilm airlift suspension reactor (BAS) and attached biomass). A three substrate-limiting model is implemented. Simplifications and assumptions, supported by experimental observation were used as shown below (Noguera et al. 1999, Wang and Zhang 2010, Beyenal and Lewandowski 2005). The model has been developed through experiments performed on a plant at lab scale and also with a sensitivity analysis. The research was developed at the Department of Civil and Environmental Engineering of the University of Rome "La Sapienza" in 2009–2010.

Materials and methods

The technological scheme

The modified BAS reactor here modelled originates from a typical deep shaft reactor (30–40 m deep, diameter $\leq$ 1 m) where an airlift is used to raise the wastewater up. The characteristic short residence times of these systems have suggested the inclusion of an attached biomass section to increase the sludge retention time, ensuring that the slowest processes will occur (e.g., nitrification–denitrification). The core of the biological treatment is thus an attached biomass section, where biomass is allowed to grow on a support constituted of rough tubular pipes, while dedicated diffusers, at different depths, assure the needed oxygen distribution through insufflated air. The suspended biomass, mainly concentrated in the deepest section of the reactor allows for a further carbonaceous substrate removal before the sludge is raised up and separated in a flotation section. This scheme thus, combines the advantages of the attached biomass systems with those derived from the adopted high pressure technique (i.e., the high dissolved oxygen concentrations that in many cases represents a limiting factor in conventional treatment processes). The solid separation by flotation allows for a further increase in the effluent quality. Finally, the proposed scheme allows a lower sludge production and a reduction of odours impacts as a consequence of the higher dissolved oxygen concentrations. A numerical model was implemented to simulate this modified BAS, whose layout is shown in Fig. 1.

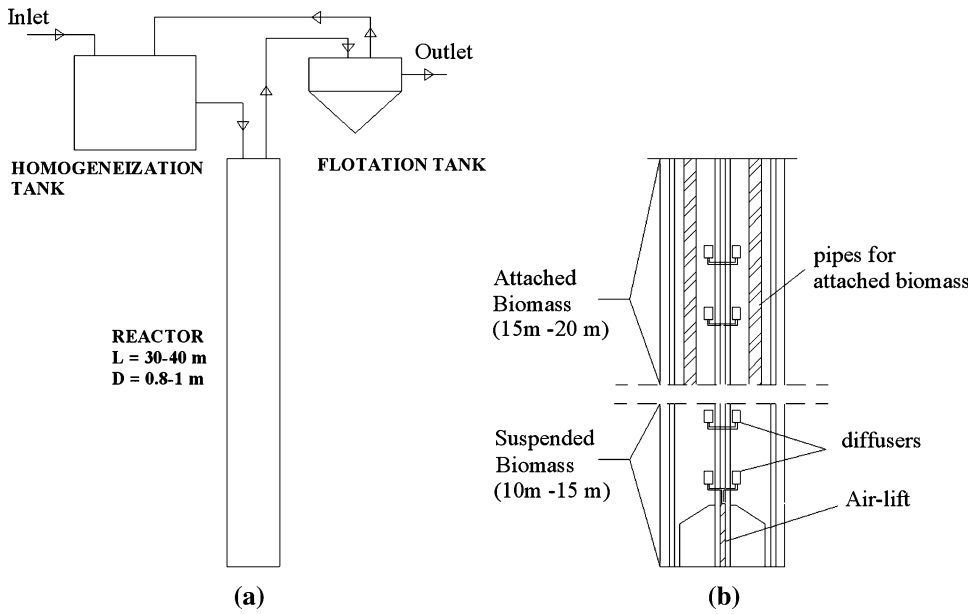

Fig. 1 Full-scale reactor scheme

Experimental set-up for model validation

The validation of the proposed model was carried out using the experimental results derived from several experiments performed on a plant at lab scale (Fig. 5) that are explained in detail in Luciano et al. (2012). The main characteristics of the experimental scheme includes:

a. a mixed homogenisation tank (DT);
b. two attached-biomass aerated reactors in series (AB1 and AB2), reproducing the upper part of the modified BAS system (working at 2 bar);
c. a suspended biomass (SB) high-pressure reactor (able to work at 2–5 bar), equipped with air diffusers, reproducing the deeper part of the modified BAS (here suspended biomasses are considered for completing the treatment) where the pressure effects on biomass was investigated;
d. a flotation tank for the solids separation of the reactor outflow (FT).

The numerical model was validated by considering the results obtained in the AB1 and AB2 reactors which represent the core of the treatment. Domestic wastewater derived from a treatment plant in Rome, collected after the grit removal section, was used as the feed (COD = 590–610 mgL^{-1}; BOD5 = 328–340 mgL^{-1}; TN = 31–66 mgL^{-1}; BOD_5/N = 5–10). The entire experiment lasted 83 days for a total of 15 runs. The microbial consortium was withdrawn from a conventional activated sludge (CAS) process and slowly acclimatized to let it grow and develop on the rough pipes supports. pH and temperature were continuously monitored in the experiments. Variations of these two parameters were considered not significant as pH ranged between 7 and 8 while temperature in the lab experiments was maintained at room temperature (approximately 20 °C).

Each run consisted of the following steps: (1) the feed stream was spiked with the substrate, (2) the system was run for a hydraulic retention time (HRT) of 4 h, and samples were collected every hour, (3) the system has been emptied and re-filled for the following run. The biofilm thickness was continuously measured with a microscope using removable supports inserted at different heights in the reactor. The COD, $N–NH_4^+$, NO_3^-, NO_2^-, and SS were determined according to standard methods (Eaton et al. 2005).

The numerical framework

The developed model was used to evaluate the overall removal efficiencies on the COD and nitrogen. Different authors have evidenced that sophisticated approaches are often not useful for the scale-up of the processes investigated at lab scale (Pizarro et al. 2001; Beyenal and Lewandowski 2005). Beyenal and Lewandowski (2005) reported that the use of a scheme based on a homogeneous—biofilm model ignores structural biofilm effects, but can be verified experimentally, whereas, heterogeneous biofilm models include the importance of biofilm structure, but are difficult to verify experimentally.

The biological model here presented is substantially based on:

– a flux model in the reactor that considers that, under steady-state conditions, the transport of the substrate occurs thanks to the convective–diffusive phenomena;

– a biofilm model that is able to evaluate the substrate utilisation rate (Saravanan and Sreekrishnan 2006), considering the transport resistances from the liquid phase to the liquid–biofilm interface (external mass transport) and the transport from the interface to the active sites of the biofilm (internal mass transport).

By integrating the set of partial differential equations, it is possible to obtain the substrates concentration profiles within the biofilm and the substrate concentrations over the reactor depth. Furthermore, knowing the amount of dissolved oxygen consumed and taking into consideration the diffusional resistances, the anoxic zone in the biofilm structure can be identified. By determining the thickness of the anoxic zones, it is possible to assess the effects of the denitrification process on the nitrates concentration. A flow chart of the model is shown in Fig. 2.

The model also takes into consideration the ratio between the microorganisms that use carbonaceous substrate (X_C) and the nitrifying microorganisms (X_N) at the different depths in the reactor by means of an empirical law derived from literature data (Matsumoto et al. 2007; Paolini 1988). The composition of the substrate (e.g., the carbon concentration expressed by the C:N ratio) has a considerable influence on the nitrification (Walter et al. 2005; Seixo et al. 2004).

$$R = \frac{C_{\mathrm{BOD}}}{C_{\mathrm{NH_4^+}}},\ X_N = X_C \times 0.2065\, R^{-0.868} \quad (1)$$

The finite difference approach (FDT) here adopted is appropriate for the hypothesized homogeneous biofilm. More complicated mechanisms do not provide additional advantages as report by Pizarro et al. (2001), who consider that cellular automata models (i.e., the most frequently used for modeling the evolution of biofilm structure) do not have other significant advantages over FDT models when the mass transport occurs perpendicular to the biofilm. The choice of an implicit scheme guarantees fast convergent solutions. The numerical solution was based on the flow chart reported in Fig. 2 using an iterative process in which the initial substrates trends were hypothesized both in the biofilm and along the reactor. The iterative process was interrupted when an error lower than 10^{-6} was achieved.

The flux model

The flux model, applied to the whole reactor, is based on the following simplifying hypotheses (La Motta and Mulcahy 1978; Eramo et al. 1994; Viotti et al. 2002):

1. The flow in the reactor can be considered to be one-dimensional;
2. The active processes in the reactor are the convective and dispersive processes;
3. The substrates are considered to be dissolved and their concentrations do not interfere with the fluid motion;
4. The biomass is present only in the attached form; therefore, the further removal effect caused from the suspended biomass is not considered in the modelling (so remaining in safety conditions);
5. The characteristics of the material in the supports are uniform in the reactor;
6. Conditions are steady state;
7. Head losses can be considered very low (negligible) due to the low velocity of the fluid (few cm s^{-1}). The pressure drops are, however, controlled by the air flux in the airlift device that controls the flow managing the mass balance of the liquid phase.

Steady-state condition can be considered applicable if different time scales are observed for the different involved processes (Klapper and Dockery 2010); the biological processes here observed operate at larger time scales as compared to the time scales of the flow. In fact, as reported by Klapper and Dockery (2010), "the usual practice is to introduce equilibrium in the fast processes: bulk fluid flow, when considered, is assumed steady over a quasi-static biofilm, and then advection–reaction–diffusion processes

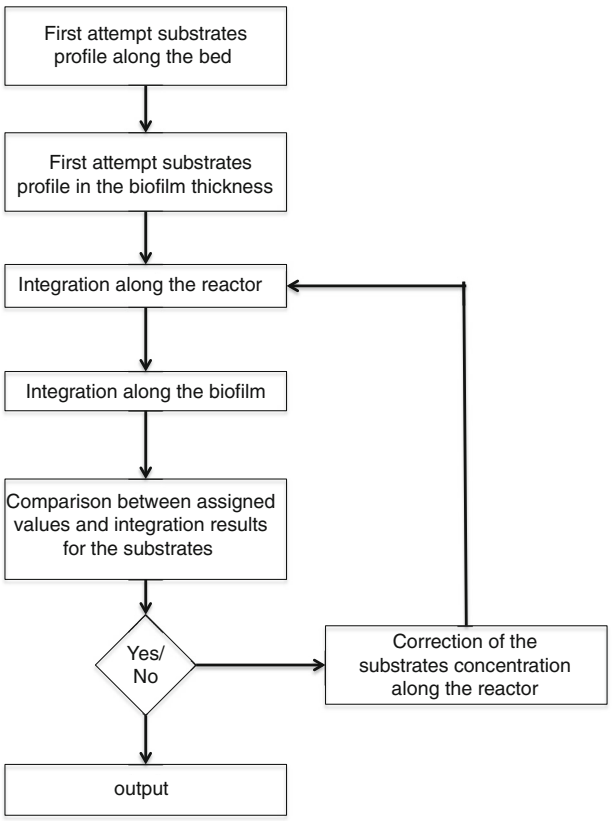

Fig. 2 Flow chart

are also assumed to be quasi-steady relative to the given fluid velocity field." The mass balance equation, which is used to model the concentration variation of each substrate in the reactor (S_b), can be written by assuming the scheme shown in Fig. 3, in which the z axes is assumed to be positive in the downward direction. Because there are typically no radial gradients in the concentration, radial dispersion has no effect and can be neglected (Devinny and Ramesh 2005).

$$u\frac{dS_b}{dz} - D_z\frac{d^2S_b}{dz^2} + R_v = 0 \quad (2)$$

The boundary conditions for the substrate mass balance equation are:

$$\begin{aligned} S_b^d &= S_b^i \quad \text{per } z = 0 \\ \frac{dS_b}{dz} &= 0 \quad \text{per } z = H_r \end{aligned} \quad (3)$$

Equation 2 can be rewritten for each substrate involved in the process (COD, NH_4^+, NO_2^-,NO_3^- and oxygen). In the present paper, however, the oxygen transport–dispersion equation along the reactor was neglected and replaced by a distribution derived by means of Henry's law. The assumption was possible because of the high contributions of air from the diffusers located along the reactor and from the air lift which allowed neglecting the oxygen limiting conditions in the bulk fluid. Furthermore, the nitrite equation is not reported in both of the models (flux model along the reactor—biofilm model), to simplify the manuscript. The substance is in fact considered as an intermediate product of ammonia oxidation/nitrate reduction.

In the following paragraph, the equations are written for a generic substrate S_b, while the specific equations are reported in Table 1 for each of the considered substrates (COD, NH_4^+, NO_3^-). The complete set of parameters used in the model equation is reported in Table 2. The Eq. 2 was adimentionalized by dividing the concentration by the inlet concentration S_b^i and by dividing z by H_r.

$$\zeta = \frac{Z}{H_r} \quad (4)$$

$$B^* = \frac{S_b}{S_b^i} \quad (5)$$

Posing:

$$\tau = \frac{H_r}{u} \quad (6)$$

and introducing $B_0 = \frac{D_z}{(uH_r)}$ as the Bodestein number:

$$\frac{dB^*}{d\zeta} - B_0\left[\left(\frac{d^2B^*}{d\zeta^2}\right)\right] + R_V\frac{\tau}{S_b^i} = 0 \quad (7)$$

With the modified boundary conditions:

$$\begin{aligned} B^* &= 1 \quad \text{per } \zeta = 0 \\ \frac{dB^*}{d\zeta} &= 0 \quad \text{for } \zeta = 1 \end{aligned} \quad (8)$$

The biofilm model

The utilization of a substrate by the microorganisms takes place through three different mechanisms (Viotti et al. 2002; Saravanan and Sreekrishnan 2008): (1) external mass transport (substrate transport from the liquid phase to the liquid-biofilm interface); (2) internal mass transfer (substrate transport from the interface to the inner part of the biofilm) and (3) substrate utilization inside the biofilm. The removal process of each substrate can be analyzed by writing the mass balance equation for the reference volume with the following assumptions (La Motta and Mulcahy 1978; Eramo et al. 1994; Viotti et al. 2002):

1. The biofilm is homogeneous and its thickness is uniform;
2. In the mass balance equation the transport process is given only by the diffusive process based on Fick's law, D is the molecular diffusion coefficient characteristic of each substrate;
3. The removal kinetic reactions are based on a multi-substrate Michaelis–Menten's law; the assumption of removal kinetics of first-order for the carbonaceous substrate has been reported in the scientific literature

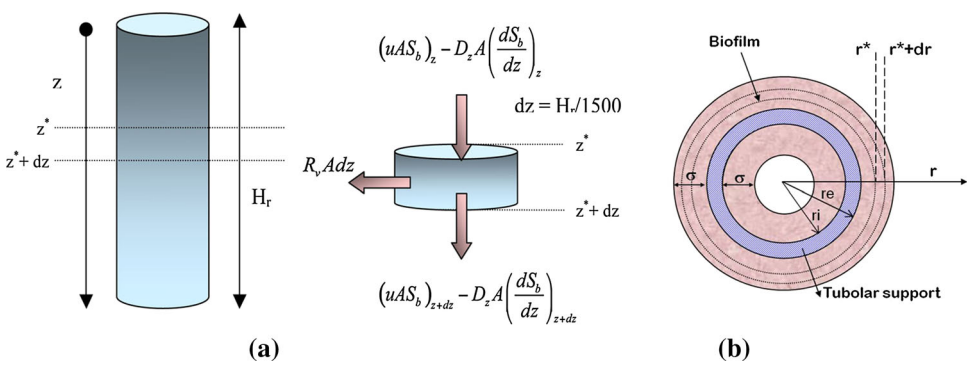

Fig. 3 Reactor (**a**) and biofilm (**b**) reference systems

Table 1 Complete set of dimensionless flux equations

Substrate	Equation	Eq.	Boundary conditions
Carbonaceous	$\frac{dB^*}{d\zeta} - B_0 \frac{d^2B^*}{d\zeta^2} + 2\eta_c \frac{V_b}{V_l} n_t \frac{\tau}{COD_b^i} K_c \rho_{bc} \frac{B^*}{Y_c + B^*} = 0$	A1	$B^* = 1$ for $\zeta = 0$ $\frac{dB^*}{d\zeta} = 0$ for $\zeta = 1$
Ammonia	$\frac{d\Lambda^*}{d\zeta} - B_0 \frac{d^2\Lambda^*}{d\zeta^2} + 2\eta_n \frac{V_b}{V_l} n_t \frac{\tau}{NH_{4b}^i} K_n \rho_{bn} \frac{\Lambda^*}{Y_n + \Lambda^*} = 0$	A2	$\Lambda^* = 1$ for $\zeta = 0$ $\frac{d\Lambda^*}{d\zeta} = 0$ for $\zeta = 1$
Nitrate	$\frac{dN^*}{d\zeta} - B_0 \frac{d^2N^*}{d\zeta^2} + 2\eta_d \frac{V_b}{V_l} n_t \frac{\tau}{NO_{3b}^i} K_d \rho_{bd} \frac{N^*}{Y_d + N^*} = 0$	A3	$N^* = 1$ for $\zeta = 1$ $\frac{dN^*}{d\zeta} = 0$ for $\zeta = 1$

and has been confirmed by the experimental results reported in Luciano et al. (2012). For the nitrification process, a removal rate between the first and the second order has been observed. By considering a multi-substrate limiting model, it is possible to take into consideration the non-linearity of the removal kinetics. This is also favoured from the different time-scales of the processes, so in the upper section of the reactor takes place mainly the removal of COD. The nitrification process is delayed by the slower kinetic and occurs at middle depths, where the DO is still available. Nitrates here produced are then removed in the deeper part of the biofilm, where small amounts of COD are still available and the DO penetration is limited both due to the high shear stresses at the liquid–biofilm interface and to its biological consumption.

4. The conditions are steady-state;
5. The supports are cylindrical and the biofilm growth occurs on both the inner and outer surfaces.

With respect to the reference system chosen for the particle (Fig. 3b), the mass balance equation for the generic substrate (S) applied on an infinitesimal biofilm thickness dr, can be written in terms of steady state conditions:

$$\frac{D_{sb}}{r}\frac{d}{dr}\left(r\frac{dS}{dr}\right) - K\rho_{bs}\frac{S}{K_s + S} = 0 \tag{9}$$

Because the convective terms are negligible, the transport in the biofilm structure is represented only by means of the diffusion term based on the Fick's law.The $S(r)$ distribution is determined by solving the above-mentioned equation once the following boundary conditions are assigned:At the biofilm–liquid bulk interface: $r = r_e + \sigma(r = r_i - \sigma)$ (Horn and Hempel 2001)

$$D_{sb}\frac{ds}{dr} = K_M(S_b - S) \tag{10}$$

At the biofilm–support interface: $r = r_e(r = r_i)$

$$\frac{ds}{dr} = 0 \tag{11}$$

The second boundary condition states that there is no-flow at the biofilm–support interface due to impermeable characteristics of the support. The first boundary condition takes into consideration the presence of an edge layer at the interface of the bulk liquid–biofilm, where the decay of the substrate is considered linear. The expression (11) states the equality between the external flux and the internal flux. The external flux is related to the concentration gradient through the mass exchange coefficient K_M. K_M can be determined using the following expression:

$$K_M = \frac{S_h D_L}{d_e + \sigma} \tag{12}$$

With the S_h being the Sherwood number (Nicolella et al. 2000):

$$S_h = 2.0 + CRe^n Sc^m \tag{13}$$

The Schmidt number (Sc) is a function of the substrate molecular diffusion in the liquid (D_L), the density (ρ) and the dynamic viscosity (μ) of the fluid:

$$Sc = \frac{\mu}{D_L \rho} \text{ Schmidt number} \tag{14}$$

The Reynolds number (Re) is defined by means of the turbulence theory, which is often used to treat fluidized bed reactors:

$$Re = \frac{\varepsilon d_s^4}{\upsilon^3} \text{ Reynold number} \tag{15}$$

ε represents the energy dissipation rate evaluated as:

$$\varepsilon = u_G g \tag{16}$$

where u_G is the gas surface velocity obtained by dividing the air flow rate by the transversal section of the reactor. In this work, the relation from Nicolella et al. (1998) is used:

$$Sh = 2 + 0.265\, Re^{0.241} Sc^{1/3} \text{ Sherwood number} \tag{17}$$

Thus,

$$K_M = \frac{S_h D_L}{d_e + \sigma} = 2 + 0.265 Re^{0.241} Sc^{\frac{1}{3}} \frac{D_L}{d_e + \sigma} \tag{18}$$

Table 2 Complete set of parameters used in the equations

Parameter	Description
$B^* = C_b/C_b^i$	COD concentration in the liquid phase in dimensionless form
$B_o = D_z/(uH_b)$	Bodenstein number (dimensionless)
C	COD concentration in the biofilm (mg L^{-1})
$C^* = C/C_b$	COD concentration in the biofilm in dimensionless form
C_b	COD concentration in the liquid phase (mg L^{-1})
C_b^d	COD concentration at the reactor (boundary cond.) (mg L^{-1})
C_b^i	COD concentration in the feed flow (boundary cond.) (mg L^{-1})
d_e	External diameter of the support (m)
d_s	Biofilm thickness plus support diameter (m)
n_t	Number of tubular supports
D^*	NO_3^- concentration in dimensionless form in the biofilm
D_L	Substrate diffusivity coefficient in the liquid phase (m^2 s^{-1})
D_{sb}	Substrate diffusivity coefficient (m^2 s^{-1})
D_{sbc}	COD diffusivity coefficient in the biofilm (m^2 s^{-1})
D_{sbn}	Ammonia–nitrogen diffusivity coefficient in the biofilm (m^2 s^{-1})
D_{sbo}	Oxygen diffusivity coefficient in the biofilm (m^2 s^{-1})
D_z	Axial dispersion coefficient (m^2 s^{-1})
H_r	Height of the attached biomass section in the reactor/length of the supports (m)
J	Substrate flux across the surface A (mg s^{-1})
K_c	COD maximum utilization rate (d^{-1})
K_n	Ammonia–nitrogen maximum utilization rate (d^{-1})
K_D	Nitrate maximum utilization rate (d^{-1})
k_{o1}	Oxygen specific consumption in the biofilm for COD degradation (kgO2 $(kgCOD)^{-1}$)
k_{o2}	Oxygen specific consumption in the biofilm for ammonia–nitrogen degradation (kgO2 $(kgNH_4^+)^{-1}$)
K_s	Half saturation constant (mg L^{-1})
K_{sc}	COD half-saturation constant (mg L^{-1})
K_{Sco}	Oxygen half-saturation constant for COD removal (mg L^{-1})
K_{Sn}	Ammonia–nitrogen half-saturation constant (mg L^{-1})
K_{Sno}	Oxygen half-saturation constant for the ammonia- nitrogen removal (mg L^{-1})
K_M	Mass exchange coefficient (m s^{-1})
N	Ammonia–nitrogen concentration in the biofilm (mg L^{-1})
$\Lambda^* = N_b/N_b^i$	Ammonia–nitrogen concentration in the reactor in dimensionless form
$N^* = N/N_b$	Ammonia–nitrogen concentration in the biofilm in dimensionless form
N_b	Ammonia–nitrogen concentration in the liquid phase (mg L^{-1})
N_b^d	Ammonia–nitrogen concentration in the reactor (boundary cond.)(mg L^{-1})
N_b^i	Ammonia–nitrogen concentration in the feed flow (boundary cond.)(mg L^{-1})
O	Oxygen concentration in the biofilm (mg L^{-1})
$O* = O/O_b$	Oxygen concentration in the biofilm in dimensionless form
O_b	Oxygen concentration in the liquid phase (mg L^{-1})
O_b^i	Oxygen concentration in the feed flow (mg L^{-1})
Q	Flow rate (m^3 s^{-1})
r	Spatial coordinate in the biofilm (m)
r_e	External radius of the support (m)
r_i	Internal radius of the support (m)
r_m	Support medium radius (m)
R	COD/NH_4^+ in the biofilm
R_e	Reynolds number

Table 2 continued

R_I	Intrinsic reaction rate for unit volume of the biofilm (kg m^{-1} s^{-1})
R_o	Observed reaction rate for unit volume of the biofilm (kg m^{-1} s^{-1})
R_v	Observed reaction rate for unit volume of the biofilm (kg m^{-1} s^{-1})
R_{vc}	Observed reaction rate for unit volume of the bed for the COD (kg m^{-1} s^{-1})
R_{vn}	Observed reaction rate for unit volume of the bed for ammonia–nitrogen (kg m^{-1} s^{-1})
S	Generic substrate concentration inside the biofilm (mg L^{-1})
S_c	Schmidt number
S_b	Generic substrate concentration in the liquid phase (mg L^{-1})
S_b^i	Substrate concentration at the inlet section (boundary cond.) (mg L^{-1})
S_b^d	Substrate concentration inside the reactor (boundary cond.) (mg L^{-1})
$u = Q/(n_t A_I)$	Fluid velocity (m s^{-1})
u_G	Gas surface velocity (m s^{-1})
$\varepsilon = u_G g$	Energy dissipation rate (m^2 s^{-3})
V_b	Biofilm volume (m^3)
V_{bi}	Internal biofilm volume (m^3)
V_{be}	External biofilm volume (m^3)
V_I	Volume of influence of a cylindrical support (m^3)
A	Area of influence of a cylindrical support (m^2)
X	(r-rm)/σ; spatial coordinate in the biofilm in dimensionless form
X_n	Nitrifying biomass concentration (mg L^{-1})
X_c	Carbonaceous biomass concentration (mg L^{-1})
Y_c	K_{sc}/C_b
Y_{co}	K_{sco}/O_b
Y_n	K_{sn}/N_b
Y_{no}	K_{sno}/O_b
Z	Spatial coordinate in the filter bed (m)
ϕ	Thiele modified module for a generic substrate
ϕ_c^2	$K_c \rho_{bd} \sigma^2/(D_{sbc} C_b)$; Thiele modified module for the COD
ϕ_{co}^2	$K_c \rho_{bd} \sigma^2/(D_{sbo} O_b)$; Thiele modified module for the oxygen in the COD removal
ϕ_n^2	$K_n \rho_{bd} \sigma^2/(D_{sbn} N_b)$; Thiele modified module for the ammonia–nitrogen
ϕ_{no}^2	$K_n \rho_{bd} \sigma^2/(D_{sbo} O_b)$; Thiele modified module for the oxygen in the ammonia–nitrogen removal
γ	K_s/S_b
γ_c	K_{sc}/C_{bi}
γ_{co}	K_{sco}/O_{bi}
γ_n	K_{sn}/N_{bi}
γ_{no}	K_{sno}/O_{bi}
η	Efficiency factor
η_c	Efficiency factor for the COD
η_n	Efficiency factor for the ammonia–nitrogen
μ	Dynamic viscosity of the liquid phase (kg m^{-1} s^{-1})
ρ	Density of the liquid phase (kg m^{-3})
ρ_{bd}	Mean biomass concentration in the biofilm (kg m^{-3})
σ	Biofilm thickness (m)
τ	H_b/u (s)
ξ	$d_m/2\sigma$
ζ	z/H_b; spatial coordinate in the bed in dimensionless form

Equation 14 must be adimentionalized and rewritten for each substrate. The radius is made dimensionless by introducing the modified x-abscissa:

$$x = \frac{r - r_e}{\sigma} = \frac{r_i - r}{\sigma} \tag{19}$$

Therefore,

$$r = \sigma x + r_e = \sigma\left(x + \frac{d_e}{2\sigma}\right) = \sigma(x + \zeta) \tag{20}$$

The substrate concentration in the biofilm is divided by the corresponding concentration in the liquid phase S_b, at the level z:

$$S^* = \frac{S}{S_b} \tag{21}$$

yielding the following:

$$\frac{D_{Sb}}{\sigma(x+\xi)}\frac{d}{\sigma dx}\left[\sigma(x+\xi)S_b\frac{dS^*}{\sigma dx}\right] - K\rho_b\frac{S^*}{\frac{K_S}{S_b} + S^*} \tag{22}$$

Posing:

$$\gamma = \frac{K_S}{S_b} \tag{23}$$

it is obtained:

$$\frac{D_{Sb}}{\sigma^2(x+\xi)}\frac{d}{dx}\left[(x+\xi)\frac{dS^*}{\sigma dx}\right] - K\rho_b\frac{S^*}{\frac{K_S}{S_b} + S^*} \tag{24}$$

Dividing by $\frac{D_{Sb}S_b}{\sigma^2(x+\xi)}$.

$$\frac{d}{x}\left[(x+\xi)\frac{dS^*}{\sigma dx}\right] - \frac{K\rho_b\sigma^2}{D_{Sb}S_b}(x+\xi)\frac{S^*}{\gamma + S^*} = 0 \tag{25}$$

using:

$$\phi^2 = \frac{K\rho_b}{D_{Sb}S_b}\sigma^2 \text{ Thiele modified module} \tag{26}$$

the final equation assumes the form:

$$\frac{d}{d_x}\left[(x+\zeta)\frac{ds^*}{dx}\right] - \phi^2(x+\zeta)\frac{S^*}{\gamma_e + S^*} = 0 \tag{27}$$

The boundary conditions for $x = 0$ and $x = 1$ are:

$$\begin{array}{ll} \frac{dS^*}{dx} = B_c(1 - S^*) & \text{for } x = 1 \\ \frac{dS^*}{dx} = 0 & \text{for } x = 0 \end{array} \tag{28}$$

where

$$B_c = \frac{K_M\sigma}{D_{Sb}} = \frac{S_h D_L}{d_m}\frac{\sigma}{D_{Sb}} \quad \text{Biot modified number} \tag{29}$$

The denitrification process

In the three substrates models, the transport and degradation equation in the biofilm is written for each substrate. The nitrification and the denitrification processes generally occur under opposite conditions (aerobic and anoxic conditions, respectively) (Hwang et al. 2005). In the wastewater treatment systems that use an attached biomass, the total balance of the nitrogen in the liquid phase is often not satisfied because anoxic conditions can occur in the deeper areas of the biofilm, allowing for the denitrification even if dissolved oxygen is still present in the liquid phase (Walters et al. 2009; Okabe et al. 1996; Satoh et al. 2004). In addition, Pochana and Keller (1999) and Puznava et al. (2001) show that the simultaneous nitrification and denitrification (SND) could occur as a consequence of the DO concentration gradients within microbial flocs or biofilms. Nitrifiers will develop on the surface of the biofilm where there are rather high DO levels, whereas denitrifiers will be present inside the biofilm due to the low levels or absence of oxygen. As a result, the effectiveness of SND is dependent on the size, density and distribution of the biofilm thickness (Pochana and Keller 1999). Studies carried out using microelectrodes show that in the case of flocs, when the diameters approach approximately 1,000–3,000 μm, nitrification and denitrification will take place in different zones of the floc (Walters et al. 2009, Satoh et al. 2003; Hille et al. 2009). Several studies have evaluated the possible performance of other treatment systems of attached biomass (Rahimia et al. 2011). For the growth of heterotrophic bacteria in the biofilm, two substrates are required, i.e., an electron acceptor (dissolved oxygen DO) and an electron donor (soluble organic matter). Both substrates are essential for bacterial growth (Wang and Wang 2012) and, consequently, the whole process is inhibited when one of the two is not available (Rauch et al. 1999). Furthermore, nitrification is adversely affected at high COD:N ratios due to the direct competition for molecular oxygen between autotrophs (nitrifying microorganisms) and heterotrophs (carbonaceous substrate based microorganisms). If the COD:N ratio significantly decreases, denitrification can be inhibited due to the deficiency of an electron donor source (Walters et al. 2009). In developing the proposed model, the penetration depth of the oxygen in the biofilm was considered by taking into consideration the amount of oxygen consumed by the removal of carbonaceous substrates and by the nitrification process along the biofilm thickness. The whole process also considers the resistances to transport from the external surface of the biofilm to the active sites (internal transport). By evaluating the oxygen and carbonaceous substrate depth penetration, the numerical model allows for the evaluation of the nitrates removal along the thickness of the attached biomass system. Although the equation used is identical for all of the substrates, in the case of nitrate, two additional limiting factors were taken into consideration: the first related to the concentration of the oxygen and the

second to the concentration of COD. The biological removal factor was then multiplied by two parameters, α and β, which are defined below (see Table 3).

Both of these two factors vary with the depth, and with the biofilm thickness. The assumed hypothesis is to describe the variations of the two parameters through a simple step function:

$$\begin{cases} \alpha = 1 & \text{if } O_2 \leq 1 \text{ mg l}^{-1} \\ \alpha = 0 & \text{if } O_2 > 1 \text{ mg l}^{-1} \end{cases} \quad (30)$$

$$\begin{cases} \beta = 0 & \text{if COD} < 0,\ 1 \text{ mg l}^{-1} \\ \beta = 1 & \text{if COD} \geq 0,\ 1 \text{ mg l}^{-1} \end{cases} \quad (31)$$

In this way, nitrate removal can occur in the biofilm layer under anoxic condition and at the same time, when the layer contains enough COD. The modified mass balance then assumes the form of equation A6 (Table 3). Concurrently, the complete equation, used to evaluate the total amount of consumed oxygen, is correlated to the amount of substrate consumption through the following equation:

$$\frac{D_{\text{Sbo}}}{r}\frac{\mathrm{d}}{\mathrm{d}r}\left(r\frac{\mathrm{d}O_2}{\mathrm{d}r}\right) - K_{\text{O1}}K_{\text{c}}\rho_{\text{bc}}\frac{COD}{K_{\text{Sc}}+COD}\frac{O_2}{K_{\text{ScO}}+O_2} - K_{\text{O2}}K_{\text{n}}\rho_{\text{bn}}\frac{\text{NH}_4^+}{K_{\text{Sn}}+\text{NH}_4^+}\frac{\text{O}_2}{K_{SnO}+\text{O}_2} = 0 \quad (32)$$

The boundary conditions are

$$O_{2\text{b}} = O_2 \quad \text{for } r = r_e + \sigma,\ r = r_{\text{i}} - \sigma \quad (33)$$

$$\frac{\mathrm{d}O_2}{\mathrm{d}r} = 0 \quad \text{for } r = r_{\text{e}}$$

Substrate utilization rate

The numerical integration of Eq. 27 over the biofilm thickness, for the three substrates, provides the concentration trends of COD, NH_4 and NO_3 inside the biofilm. By knowing the concentration profiles, it is possible to obtain the average rate of substrate utilization per unit volume of the biofilm, R_o that represents the observed reaction rate:

Considering a biofilm that is external to the support, it is:

$$R_{\text{o}} = \frac{\int_{r_{\text{e}}}^{r_{\text{e}}+\sigma} K\rho_{\text{bd}}\frac{S}{K_{\text{S}}+S}2\pi r z dr}{V_{\text{b}}} \quad (34)$$

R_o is related to the intrinsic rate R_I by means of an efficiency factor η ($\eta < 1$). The efficiency factor is the ratio between the effective rate of substrate consumption and the rate that would be observed if, in the whole biofilm, the substrate concentration is equal to the liquid phase concentration: therefore, there is an absence of diffusional resistances at the interface and in the biofilm (S_b) (Eramo et al. 1994).

$$R_{\text{o}} = \eta R_{\text{I}} \quad (35)$$

where

$$R_{\text{I}} = K\rho_{\text{b}}\frac{S_{\text{b}}}{K_{\text{S}}+S_{\text{b}}} \quad (36)$$

The term R_v appears in the transport equation of the reactor. This term represents the reaction rate for the reactor unit volume. R_v it is obtained by multiplying R_o with the ratio of the biofilm's volume and the influence volume of the cylindrical support (V_I): where V_b = biofilm's volume (m^3) ($V_b = V_{bi} + V_{be}$)

$$V_{\text{bi}} = \pi\left[r_i^2 - (r_i - \sigma)^2\right]H_{\text{r}} \quad (37)$$

$$V_{\text{bi}} = \pi\left[(r_{\text{e}} + \sigma) - (r_{\text{e}}^2)\right]H_{\text{r}}$$

Therefore, the total R_v will be:

$$R_{\upsilon} = R_{\text{o}}\frac{V_{\text{b}}}{V_{\text{I}}}n_{\text{t}} \quad (38)$$

$$R_{\upsilon} = \eta R_{\text{I}}\frac{V_{\text{b}}}{V_{\text{I}}}n_{\text{t}} \quad (39)$$

Substituting the expression obtained for R_v, the transport equation in the reactor becomes:

$$u\frac{dS_b}{dz} - D_z\frac{d^2S_b}{dz^2} + \eta\frac{V_b}{V_I}n_t K\rho_b\frac{S_b}{K_s+S_b} = 0 \quad (40)$$

For the generic substrate S_b, R_I is always obtained from equation 36:

By adimensionalization:

$$R_{\text{I}} = K\rho_{\text{b}}\frac{\frac{S_{\text{b}}}{S_{\text{b}}^i}}{\frac{K_{\text{S}}}{S_{\text{b}}^i}+\frac{S_{\text{b}}}{S_{\text{b}}^i}} \quad (41)$$

Thus finally for the COD

$$R_{\text{IC}} = K_{\text{C}}\rho_{\text{bC}}\frac{B^*}{Y_{\text{e}}+B^*} \quad (42)$$

where

$$Y_{\text{C}} = \frac{K_{\text{SC}}}{C_{\text{b}}} \quad (43)$$

The COD transport equation then becomes:

$$\frac{\mathrm{d}B^*}{\mathrm{d}\zeta} - B_O\frac{\mathrm{d}^2B^*}{\mathrm{d}\zeta^2} + \eta_{\text{S}}\frac{V_{\text{b}}}{V_{\text{I}}}n_{\text{t}}\frac{\tau}{S_{\text{bi}}}K_{\text{S}}\rho_{\text{bS}}\frac{B^*}{Y_{\text{S}}+B^*} \quad (44)$$

where $\tau = \frac{H_r}{u}$.

and $u = \frac{Q/n_t}{A_I}$, $\frac{Q}{n_t}$ = the flow in the influence volume of a single support

An analogous treatment can be derived for the other involved substrates.

Results and discussion

Sensitivity tests analysis

In the following paragraphs are reported the sensitivity tests where are used typical inlet values of a wastewater of 5,000 inhabitants (COD = 252 mgL^{-1}, NH_4^+ = TN = 33 mgL^{-1}, NO_3^- = 0 mgL^{-1}, DO ≤ 1 mgL^{-1}, Q = 14 Ls^{-1}, length of tubular support = 15 m, nt = 20, internal reactor diameter = 0.86 m, total reactor length = 30 m).

Sensitivity tests were carried out to determine the influence of each parameter on the process. The sensitivity analysis was carried out by considering the typical dimensions of a plant at full scale (H_r, D). Table 4 reports the results for the different parameters studied in the sensitivity analysis.

The results show that the diffusivity essentially does not influence the overall removal rate. The same conclusion can be drawn for the amounts of insufflate air (air lift and air for the biological reactions).

Figure 4 reports the numerical results of some of the simulations carried out in the sensitivity analysis with different biofilm thicknesses (being constant the thickness along all the tubular supports). Graphs of the substrates trend inside the biofilm thickness at different reactor depths are presented to evidence the effects of biofilm stratification, due to the contemporary partial penetration of the substrates (COD, DO, NH_4^+), and the fate of the secondary substrates (NO_3^- in this case). The graphs are the results of the combined action of the processes (carbonaceous substrate oxidation, nitrification, denitrification and DO consumption) obtained from the numerical model.

Reference conditions

The considered reference conditions (flow rate, inlet concentrations and dimensions) were chosen to represent a plant at full-scale designed for 5,000 inhabitants (Table 5). Some of the operating parameters (biofilm thickness, COD, NH_4^+ utilization rate) were derived from experiments (Luciano et al. 2012). Other values are obtained from the results of several authors (Horn and Morgenroth 2006; Beccari et al. 1993, Characklis and Marshall 1989; Metcalf and Eddy 2003). The results of the simulation using the reference conditions are shown in Fig. 4 (σ = 1,000 μm). The figure shows the substrates profiles resulting from the integration of the set of equations (COD, NH_4, NO_3, NO_2) along the reactor (Fig. 4e–g) and along the biofilm thickness (Fig. 4a–d) for three different reactor depths (5, 10, 15 m) and for the different substrates. The sensitivity tests have been performed considering the absence of nitrates at the inlet; the nitrates are only generated from the nitrification process along the reactor while the mass balance carried out on the total nitrogen (TN) shows the effect of the denitrification that occurs in the layered biofilm. The COD removal percentage is high and equal to 94.4 % (252 mgL^{-1}inlet–14.2 mgL^{-1}outlet), ammonia was partially removed (56.7 %, 33 mgL^{-1}inlet–14.29 mgL^{-1} outlet), while the nitrates removal percentage is limited and equal to 26.7 % (33 mgL^{-1}inlet–24.7 mgL^{-1}outlet). Along the reactor (Fig. 4g), it is possible to observe the modelled nitrates production deriving from the nitrification process. The concentration of the dissolved oxygen in the bulk liquid is calculated by using Henry's law. The oxygen consumption is related to the substrate's degradation. From the results, it is observed that the oxygen penetration into the biofilm (σ = 1,000 μm) in the first part of the reactor (5 m depth) is 200 μm (Fig. 4d, 5 m); the remaining part of the biofilm can then be considered to be under anoxic conditions. In the first meters of the reactor, the oxygen consumption is higher due to the high concentrations of the substrates (COD and NH_4). However, at depths of 10 m (penetration depth of 400 μm, Fig. 4d, 10 m) and 15 m (penetration depth of 800 μm, Fig. 4d, 15 m), the oxygen consumption is limited because the carbonaceous and nitrogen substrates are diminished. When the COD concentration in the deeper part of the reactor can be considered null (Fig. 4a, 15 m), and the oxygen penetration in the biofilm is high (Fig. 4d, 15 m), the denitrification process does not occur (Fig. 4c, 15 m); therefore, the nitrates transformation takes place mainly in the higher region of the reactor (Fig. 4c, 5 and 10 m).

Biofilm thickness variation

Three different values of biofilm thickness were analyzed:

- σ = 100 μm
- σ = 500 μm
- σ = 1 mm (reference condition)

For σ = 500 μm and σ = 1 mm, the penetration of the COD substrate into the biofilm in the upper region of the reactor is equivalent (500 and 510 μm, Fig. 4a) to a similar removal efficiency even if there is a significant difference in the thickness (Fig. 4e). This behaviour is due to the dependence of the rate of substrate utilization per unit volume of the reactor with the efficiency factor, which diminishes with the thickness of the biofilm because of an increase in the diffusional resistance. However, the efficiency factor also depends on the biofilm volume, which increases with the thickness. Therefore, two mechanisms that can be

Table 3 Complete set of dimensionless transport equations along the biofilm thickness

Substrate	Equation	Eq	Boundary condition
COD	$\frac{\mathrm{d}}{\mathrm{d}x}\left[(x+\xi)\frac{\mathrm{d}C^*}{\mathrm{d}x}\right] - \phi_c^2(x+\xi)\frac{C^*}{\gamma_c+C^*} = 0$	A4	$\frac{\mathrm{d}C^*}{\mathrm{d}x} = B_{cc}(1-C^*)$ for $x=1$ $\frac{\mathrm{d}C^*}{\mathrm{d}x} = 0$ for $x=0$
NH_4^+	$\frac{\mathrm{d}}{\mathrm{d}x}\left[(x+\xi)\frac{\mathrm{d}N^*}{\mathrm{d}x}\right] - \phi_n^2(x+\xi)\frac{N^*}{\gamma_n+N^*} = 0$	A5	$\frac{\mathrm{d}N^*}{\mathrm{d}x} = B_{cn}(1-N^*)$ for $x=1$ $\frac{\mathrm{d}N^*}{\mathrm{d}x} = 0$ for $x=0$
NO_3^-	$\frac{\mathrm{d}}{\mathrm{d}x}\left[(x+\xi)\frac{\mathrm{d}D^*}{\mathrm{d}x}\right] - \alpha\beta\phi_d^2(x+\xi)\frac{D^*}{\gamma_d+D^*} = 0$	A6	$\frac{\mathrm{d}D^*}{\mathrm{d}x} = B_{cd}(1-D^*)$ for $x=1$ $\frac{\mathrm{d}D^*}{\mathrm{d}x} = 0$ for $x=0$
O_2	$\frac{\mathrm{d}}{\mathrm{d}x}\left[(x+\xi)\frac{\mathrm{d}O^*}{\mathrm{d}x}\right] - K_{o1}\phi_{co}^2(x+\xi)\frac{C^*}{\gamma_c+C^*}\frac{O^*}{\gamma_{co}+O^*} - K_{o2}\phi_{no}^2(x+\xi)\frac{N^*}{\gamma_n+N^*}\frac{O^*}{\gamma_{no}+O^*} = 0$	A7	$O^* = 1$ for $x=1$ $\frac{\mathrm{d}O^*}{\mathrm{d}x} = 0$ for $x=0$

considered to oppose one another act on the removal rate: the efficiency factor and the biofilm volume. When considering the ratio between the substrate utilization rates, when the biofilm thickness is 500 μm and 1 mm, respectively, the efficiency factor is halved, but the biofilm volume doubles, so the degree of removal is practically the same (Fig. 4e). When the thickness is larger than 1 mm, the efficiency factor decreases due to the high thickness of the biofilm, but the volume increases so much that the net result is a higher removal. When the thickness of the biofilm is small, the biofilm is completely penetrated and the whole film depth participates to the removal process. Due to the small volume involved on the support, however, the overall efficiency is lower. For the dissolved oxygen trend with a larger biofilm thickness, the presence of anoxic zones in the biofilm can be observed until a depth of 10 m (Fig. 4d, 5 and 15 m, thickness of 500 μm and 1 mm), whereas for a smaller biofilm thickness (100 μm), the oxygen can completely penetrate the biofilm depth, preventing the formation of anoxic layers along the whole reactor length and therefore practically inhibiting the nitrates removal process. As mentioned above, the COD profile along the reactors for biofilm thicknesses of 500 μm and 1,000 μm are practically identical due to the overall behaviour related to the biofilm penetration. More significant differences can be observed in the case of NH_4, where, due to the slower rate of the nitrifying bacteria, the biofilm thickness plays an important role. In the case of the greater biofilm thicknesses, in the inner biofilm where COD is not penetrated the nitrification process mainly occurs, as it can also be observed from the higher value of nitrates generated from the process (Fig. 4g). The balance of the TN evidences the effect of the denitrification process, which is limited to the higher biofilm thicknesses and shallower depths in the reactor.

COD inlet variation

The tests on the variation of the COD inlet concentration were carried out to verify the influence of this parameter on the nitric nitrogen removal because, together with the anoxic condition, it is one of the limiting factors of the denitrification phase. In this case, the values assigned to the different tests were:

- $COD_{bi} = 252$ mgL^{-1} (reference condition)
- $COD_{bi} = 600$ mgL^{-1}
- $COD_bi = 100$ mgL^{-1}

It is well known that the COD plays an important role in the denitrification process. With an inlet concentration equal to 100 mgL^{-1} at a reactor depth of 5 m, the COD concentration is equal to 15 mgL^{-1}, and due to the presence of the dissolved oxygen at this depth there are no anoxic zones. Thus, the denitrification is limited to the first 4.5 m of the reactor. If, however, the COD concentration at the inlet is equal to 600 mgL^{-1}, at a depth of 5 m, the thickness of the anoxic zone is greater than that under the reference condition because the oxygen consumption is larger. In combination with high volumetric loading rates, high C:N ratios lead to a noticeable decrease in the nitrification rate. Therefore, the competition for the available oxygen shifts the balance within the biofilm, favouring the denitrifying bacteria (Walter et al. 2005); this result should be considered also when evaluating the recirculation ratio.

Nitrogen inlet variation

The tests were carried out with the following boundary conditions:

- $NH_{4i} = 33$ mgL^{-1} (reference condition)
- $NH_{4i} = 60$ mgL^{-1}
- $NH_{4i} = 15$ mgL^{-1}

By varying the inlet concentration, it is possible to observe a small variation in the removal efficiency. This effect can be attributed to two superimposed phenomena: the flow velocity (which defines the HRT); and the ratio between the autotrophic and heterotrophic biomasses.

From the results, as evidenced in the next section, it can be deduced that the flow velocity is the most influent parameter on the performances of the process.

Table 4 Sensitivity analysis results (* Reference conditions)

Parameter	Parameter variation	Removal efficiency (%)			Sensitivity (%)		
		COD	NH_4	TN	COD	NH_4	TN
Biofilm	$\sigma = 100$ μm	54.3	5.9	0.2	−42.5	−89.6	−99.4
	$\sigma = 500$ μm	94.2	29.3	13.9	−0.2	−48.4	−46.1
	$\sigma = 1{,}000$ μm (*)	94.4	56.7	25.7	0.0	0.0	0.0
COD inlet	100 mg l^{-1}	96.8	82.8	14.9	2.6	46.1	−41.9
	252 mg l^{-1}(*)	94.4	56.7	25.7	0.0	0.0	0.0
	600 mg l^{-1}	54.3	5.9	0.2	−42.5	−89.6	−99.4
NH_4 inlet	15 mg l^{-1}	94.4	59.2	39.4	0.0	4.5	53.1
	33 mg l^{-1}(*)	94.4	56.7	25.7	0.0	0.0	0.0
	60 mg l^{-1}	94.4	53.7	15.2	0.0	5.2	−41.0
Flowrate	7 l s^{-1}	99.9	91.9	28.9	5.9	62.2	12.2
	14 l s^{-1}(*)	94.4	56.7	25.7	0.0	0.0	0.0
	42 l s^{-1}	53.4	19.4	8.0	−43.5	−65.8	−69.0

Flow variation

Two further values of the flow rate were evaluated to determine how the model would respond to the variation in such an important parameter. The flow velocity surely influences the HRT and the diffusional resistances at the biofilm–bulk liquid interface (Vieira and Melo 1999). Generally, a high turbulence (high Reynolds number) favours the mass transfer at the interface between the biofilm and bulk liquid, thereby allowing for a better penetration of the substrates, but at the same time the HRT diminishes (obviously neglecting a possible recycle), and this cause the reduction in the overall degree of removal.

Model validation

The proposed model was validated by means of several simulations based on the experimental results derived from the lab-scale reactor described in "Experimental set-up for model validation". A detailed description of the experimental results is reported in Luciano et al. 2012. The parameters used for the simulations are the same as those reported in Table 5, except for the reactor dimensions and biofilm thickness. Figure 5 shows the comparisons of three different experimental runs, for which different biofilm thickness were considered. Samples during the experiments were collected in time in a re-circulating reactor (corresponding to a reactor with a length of 5 m). Due to the steady state conditions of the tests, the samples can be considered distributed over the space (reactor length). In Fig. 5, space was added as a secondary abscissa (using the flux velocity, 0.00034 ms^{-1},in the experiments as the conversion factor) to avoid any doubt. The model correctly predicts the experimental data, which showed an increase in the COD removal with an increase in biofilm thickness (Fig. 5a, c). Thicker biofilms (Fig. 5c, d) showed increases in removal efficiencies for both of the substrates, even if higher volumes of attached biomass reveal the effects caused by the diffusional resistance inside the biofilm that limited the COD and oxygen penetration. The results in terms of COD and NH_4^+ trends in the reactor demonstrate the capability of the model to reproduce the experimental behaviour of the reactor in all the three tests with different biofilms thicknesses.

Conclusion

The numerical model presented in this work is able to properly simulate the removal of the different substrates in a new and alternative wastewater treatment system with high efficiencies, low volumes requirement and low odour impact. The model can be considered an intermediate level between more sophisticated models (in terms of biomasses description) and simpler models, and can therefore represents a valid tool for plant design and optimal management strategy. In the case of a weak organic load in the wastewater, an exhaustive (in-depth) study on the biomasses does not really enhance the results with particular regard to the efficiencies values that represent, from a design perspective, the most important parameter for the optimal sizing of the treatment sections. The model demonstrates the influence of the hydrodynamic and biological processes on the substrate removal efficiency. The results indicate that the most important parameter in order to obtain an excellent treatment is the biofilm thickness. A thicker biofilm does not offer great advantages in terms of carbonaceous substrate removal, but it may play an important role in nitrogen treatment. A large biofilm thickness can allow for nitrification as well as denitrification in the deeper part of the biofilm layers; the simultaneous nitrification/denitrification

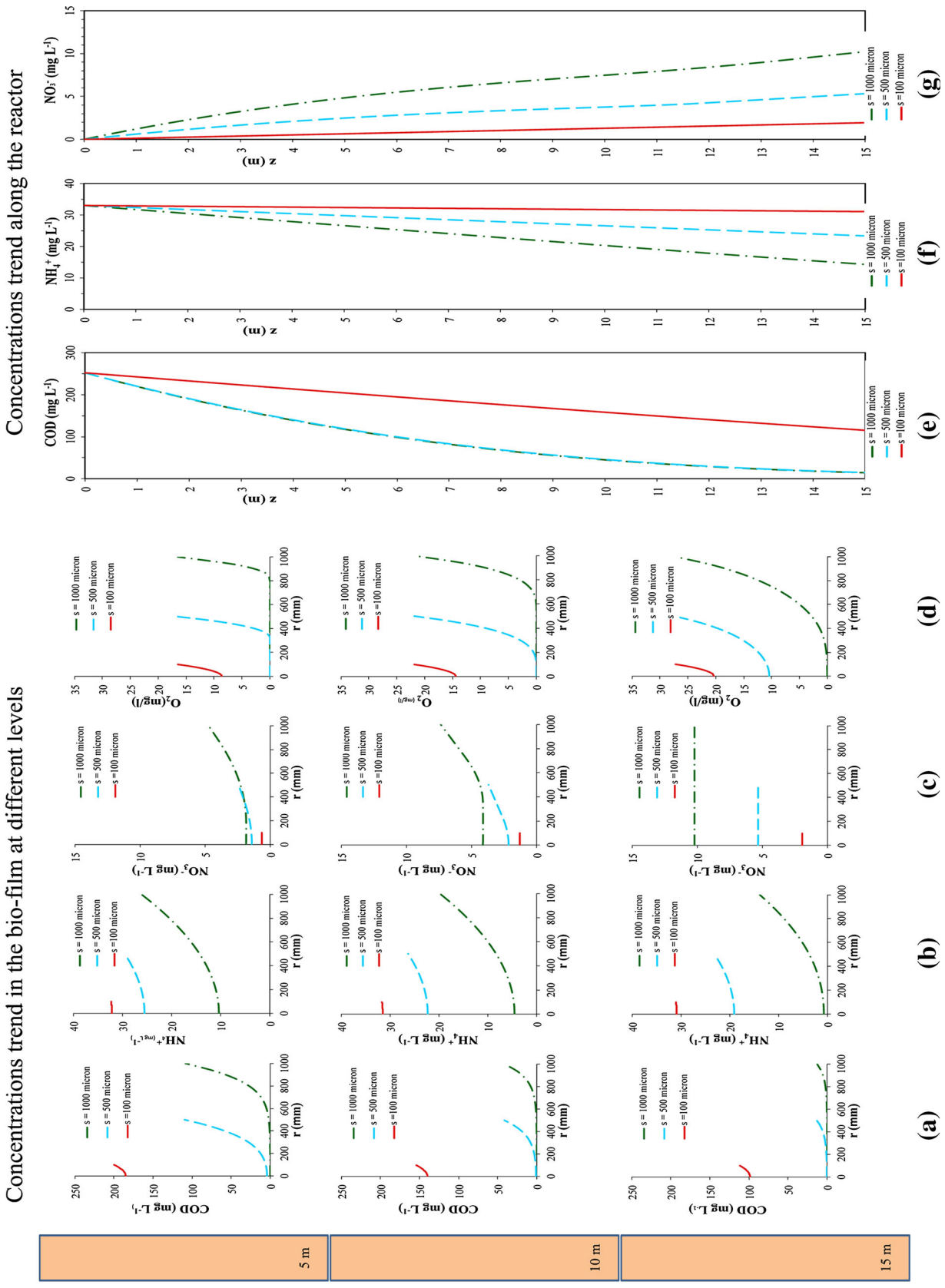

Fig. 4 Results of simulation for the reference conditions and for different biofilm thickness. **a–d** Substrates profiles inside the biofilm, **e–g** substrates profiles along the reactor

Table 5 Reference parameters used in the simulation

Parameter	Name	Value	Units		Ref.
Liquid density	R	998	kg m^{-3}	Cost.	Characklis and Marshall (1989)
Liquid dynamic viscosity	M	1.005×10^{-3}	kg m^{-1} s^{-1}	Cost.	Characklis and Marshall (1989)
Reactor diameter	D	0.844	M	Cost.	
Reactor height	H	15	M	Cost.	
Support pipes (number)	n_t	20		Cost.	
Pipe external diameter	D_e	0.090	M	Cost.	
Pipe internal diameter	D_i	0.081	M	Cost.	
Air-lift diameter		0.127	M	Cost.	
Flow-rate	Q	14	L s^{-1}	Var.	
COD inlet	COD_{in}	252	mg L^{-1}	Var.	
NH_4^+ inlet	$NH_4^+{}_{in}$	33	mg L^{-1}	Var.	
COD liquid diffusivity	D_{SLC}	1.28×10^{-9}	m^2 s^{-1}	Cost.	Tucker and Nelken (1982)
NH_4^+ liquid diffusività	D_{SLN}	1.7×10^{-9}	m^2 s^{-1}	Cost.	Characklis and Marshall (1989)
NO_2^- liquid diffusivity	D_{SLNO2}	$1.55 \cdot 10^{-9}$	m^2 s^{-1}	Cost.	Tucker and Nelken (1982)
NO_3^- liquid diffusivity	D_{SLNO3}	1.55×10^{-9}	m^2 s^{-1}	Cost.	Tucker and Nelken (1982)
Oxygen liquid diffusivity	D_{SLO}	2.44×10^{-9}	m^2 s^{-1}	Cost.	Characklis and Marshall (1989)
COD diffusivity in the biofilm	D_{SBC}	1.02×10^{-9}	m^2 s^{-1}	Var.	Characklis and Marshall (1989)
NH_4^+ diffusivity in the biofilm	D_{SBN}	1.30×10^{-9}	m^2 s^{-1}	Var.	Characklis and Marshall (1989)
NO_2^- diffusivity in the biofilm	D_{SBNO2}	1.40×10^{-9}	m^2 s^{-1}	Var.	Piciorenau et al. (2004)
NO_3^- diffusivity in the biofilm	D_{SBNO3}	1.40×10^{-9}	m^2 s^{-1}	Var.	Piciorenau et al. (2004)
Oxygen diffusivity in the biofilm	D_{SBO}	2.20×10^{-9}	m^2 s^{-1}	Var.	Piciorenau et al. (2004)
COD maximum utilization rate	k_C	10.0	d^{-1}	Cost.	Luciano et al. (2012)
NH_4^+ maximum utilization rate	k_N	4.8	d^{-1}	Cost.	Luciano et al. (2012)
NO_2^- maximum utilization rate	k_{NO2}	0.2	d^{-1}	Cost.	Metcalf and Eddy (2003)
Half-saturation constant (COD)	K_{Sc}	30	mgL^{-1}	Cost.	Metcalf and Eddy (2003)
Half-saturation constant (NH_4^+)	K_{Sn}	1	mgL^{-1}	Cost.	Metcalf and Eddy (2003)
Half-saturation constant (NO_2^-)	K_{Sno2}	0.1	mgL^{-1}	Cost.	Metcalf and Eddy (2003)
Half-saturation constant (O_2/COD)	K_{Sco}	4×10^{-4}	kg m^{-3}	Cost.	Borden and Bedient (1986)
Half-saturation constant (O_2/NH_4^+)	K_{Sno}	4×10^{-4}	kg m^{-3}	Cost.	van Haandel and van der Lubbe (2007)
Oxygen consumption for NH_4^+	k_{o3}	4.57	kgO_2 m^{-3}	Cost.	Characklis and Marshall (1989)
Oxygen consumption for the COD removal	k_{o4}	1.07	kgO_2 $(kgCOD)^{-1}$	Cost.	Characklis and Marshall (1989)
Heterotrophic biomass density	ρ_{bdh}	60	kgVSS m^{-3}	Var.	Beccari et al. (1993)
Autotrophic biomass density	ρ_{bda}	20	kgVSS m^{-3}	Var.	Beccari et al. (1993)
Axial dispersion coefficient	D_z	1×10^{-4}	$m^2 s^{-1}$	Cost.	Characklis and Marshall (1989)
Temperature	T	12	C	Cost.	
pH		7.2		Cost.	
T corr. coef. for the max. utilization rate (COD)		1.035		Cost.	Metcalf and Eddy (2003)
T corr. coef. for the max. utilization rate (NH_4^+)		1.123		Cost.	Metcalf and Eddy (2003)
T corr. coef. for the max. utilization rate (NO_2^-)		1.08		Cost.	Metcalf and Eddy (2003)
pH corr. coef. for the max. utilization rate (NH_4)		0.833		Cost.	Metcalf and Eddy (2003)

processes can also be regulated from the amount of available carbonaceous substrates and from the oxygen penetration into the biofilm. The diffusional resistances at the biofilm/bulk liquid interface are important; an increment of the flow velocity, improves the mass transfer between the bulk liquid and the internal biofilm because of the increase of turbulence but, at the same time, can induce a drastic reduction in the overall removal efficiency due to the reduction in the hydraulic residence time. It should be noted as the presented model was used for the design of treatment plant at a full-scale in deep shaft reactor currently operating in Italy (Abbadia San Salvatore, SI).

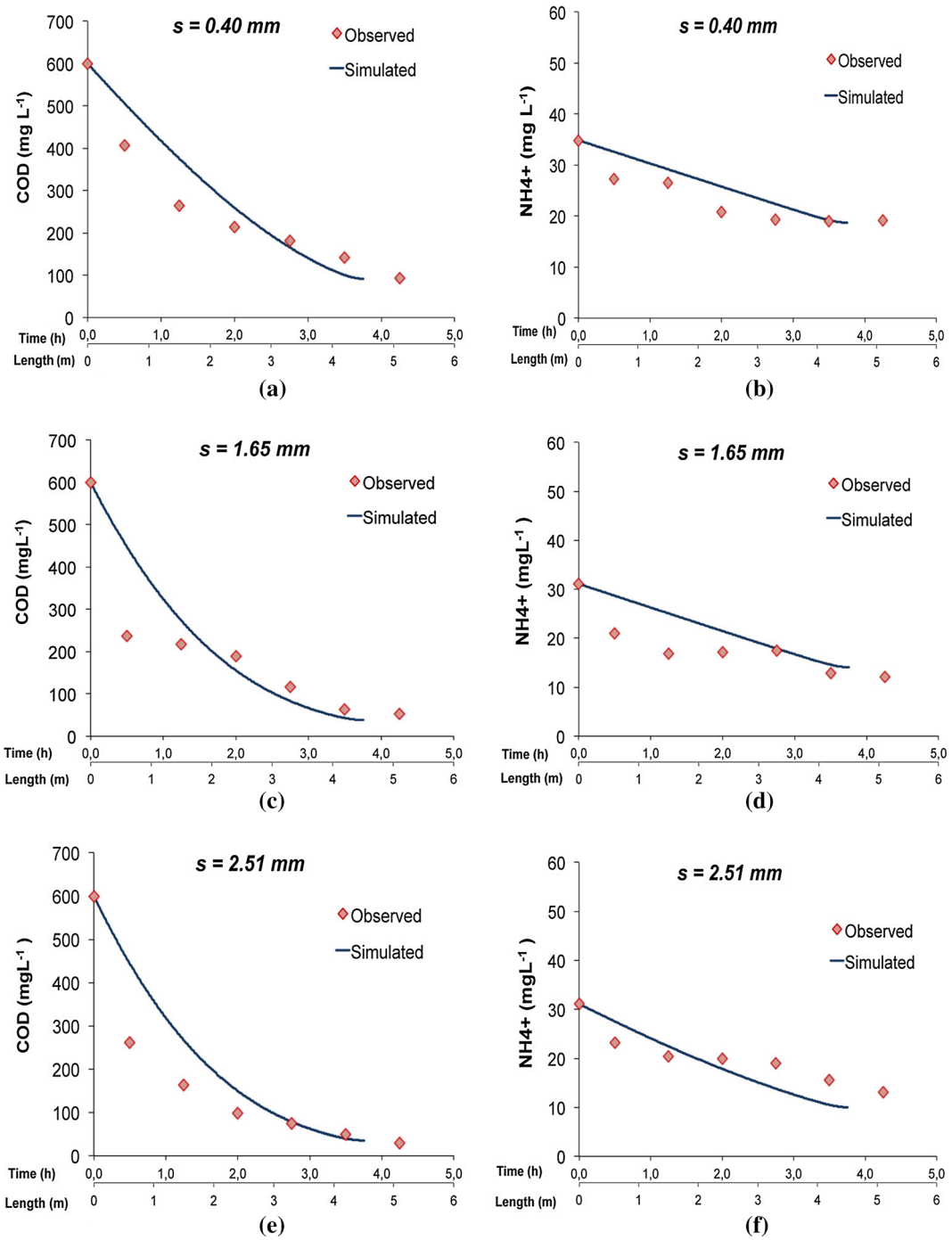

Fig. 5 Observed and simulated COD and NH_4^+ concentration trend for different biofilm thickness

Acknowledgments We gratefully acknowledge P&M Srl for providing data information for the design at full scale.

References

Akhbari A, Zinatizadeh AAL, Mohammadi P, Mansouri Y, Irandoust M, Isa MH (2012) Kinetic modeling of carbon and nutrients removal in an integrated rotating biological contactor-activated sludge system. Int J Environ Sci Technol 9(2):371–378

Beccari M, Passino R, Ramadori R, Vismara R (1993) Rimozione di Azoto e Fosforo dai Liquami. Hoepli, Italy

Beyenal H, Lewandowski Z (2005) Modeling mass transport and microbial activity in stratified biofilms. Chem Eng Sci 60:4337–4348

Borden RC, Bedient PB (1986) Transport OD dissolved hydrocarbons influenced by oxygen-limited biodegradation 1. Theoretical development. Water Res 22(13):1973–1982

Characklis WG, Marshall KC (1989) Biofilms. Wiley Interscience, New York

Devinny JS, Ramesh J (2005) A phenomenological review of biofilter models. Chem Eng J 113:187–196

Eaton AD, APHA, AWWA, WEF (2005) Standard methods for the examination of water and wastewater. 21st edn. American Public health Association, Washington, DC

Eramo B, Gavasci R, Misiti A, Viotti P (1994) Validation of a multisubstrate mathematical model for the simulation of the denitrification process in fluidized bed biofilm reactors. Water Sci Technol 29(10–11):401–408

De Feo (2007) Carbon and nitrogen removal from low-strength domestic wastewater with a two-stage submerged biological filter. J Environ Sci Health A Tox Hazard Subst Environ Eng 42(5):641–647

Harremoës P (1976) The significance of pore diffusion to filter denitrification. J Water Pollut Con F 48:377–388

Hille A, Mei HE, Ochmann C, Neu TR, Horn H (2009) Application of two component biodegradable carriers in a particle-fixed biofilm airlift suspension reactor: development and structure of biofilms. Bioprocess Biosyst Eng 32:31–39

Horn H, Hempel DC (2001) Simulation of substrate conversion and mass transport in biofilm systems. Eng Life Sci 1(6):225–228

Horn H, Morgenroth E (2006) Transport of oxygen, sodium chloride, and sodium nitrate in biofilms. Chem Eng Sci 61:1347–1356

Hwang YW, Kim CG, Choo IJ (2005) Simultaneous nitrification/denitrification in a single reactor using ciliated columns packed with granular sulfur. Water Qual Res J Can 40(1):91–96

Jiang F, Leung DH-W, Li S, Chen G-H, Okabe S, van Loosdrecht MCM (2009) A biofilm model for prediction of pollutant transformation in sewers. Water Res 43:3187–3198

Klapper I, Dockery J (2010) Mathematical description of microbial biofilms. Siam review. Soc Ind Appl Math 52(2):221–246

La Motta EJ, Mulcahy LT (1978) Mathematical model of the fluidized bed biofilm reactor. Department of Civil Engineering, University of Massachusetts, Amherst. Report No Env: E 59–78

Luciano A, Viotti P, Mancini G, Torretta V (2012) An integrated wastewater treatment system using a bas reactor with biomass attached to tubular supports. J Environ Manag 113:51–60

Matsumoto S, Terada A, Tsuneda S (2007) Modeling of membrane-aerated biofilm: effects of C/N ratio, biofilm thickness and surface loading of oxygen on feasibility of simultaneous nitrification and denitrification. Eng J 37:98–107

Metcalf and Eddy 2003. Wastewater engineering: treatment and reuse. 4th edn, McGraw Hill, New York, pp 1819

Morgenroth E, Eberl HJ, van Loosdrecht MCM, Noguera DR, Pizarro GE, Picioreanu C, Rittmann BE, Schwarz AO, Wanner O (2004) Comparing biofilm models for a single species biofilm system. Water Sci Technol 4:145–154

Mudliar S, Banerjee S, Vaidya A, Devotta S (2008) Steady state model for evaluation of external and internal mass transfer effects in an immobilized biofilm. Bioresour Technol 99:3468–3474

Nicolella C, van Loosdrecht MCM, Heijnen JJ (1998) Mass transfer and reaction in a biofilm airlift suspension reactor. Chem Eng Sci 53(15):2743–2753

Nicolella C, van Loosdrech MCM, Heijnene SJ (2000) Particle-based biofilm reactor technology. Trends Biotechnol 18(7):312–320

Noguera DR, Okabe S, Picioreanu C (1999) Biofilm modeling: present status and future directions. Water Sci Technol 39(7):273–278

Okabe S, Hiratia K, Ozawa Y, Watanabe Y (1996) Spatial microbial distributions of nitrifiers and heterotrophs in mixed-population biofilms. Biotechnol Bioeng 50:24–35

Paolini AE (1988) Lezioni di trattamento degli effluenti industriali. Ed. Siderea

Piciorenau C, Kreft JU, van Loosdrecht MCM (2004) Particle-based multidimensional multispecies biofilm model. Appl Environ Microbiol 70(5):3024–3040

Pizarro G, Griffeath D, Noguera DR (2001) Quantitative cellular automaton model for biofilm. J Environ Eng ASCE 127:782–889

Pochana K, Keller J (1999) Study of factors affecting simultaneous nitrification and denitrification (SND). Water Sci Technol 39(6):61–68

Puznava N, Payraudeau M, Thornberg D (2001) Simultaneous nitrification and denitrification in biofilters with real time aeration control. Water Sci Technol 43(1):269–276

Rahimia Y, Torabiana A, Mehrdadia N, Shahmoradib B (2011) Simultaneous nitrification–denitrification and phosphorus removal in a fixed bed sequencing batch reactor (FBSBR). J Hazard Mater 185:852–857

Rahman NK, Bakar MZA, Uzir MH, Kamaruddin AH (2009) Modelling on the effect of diffusive and convective substrate transport for biofilm. Math Biosci 218:130–137

Rauch WM, Vanhooren H, Vanrolleghem PA (1999) A simplified mixed-culture biofilm model. Water Res 33(9):2148–2162

Rittmann BE, McCarty PL (1980) Evaluation of steady-state-biofilm kinetics. Biotechnol Bioeng 22(11):2359–2373

Russo ME, Maffettone PL, Marzocchella A, Salatino P (2008) Bifurcational and dynamical analysis of a continuous biofilm reactor. J Biotechnol 135:295–303

Saravanan V, Sreekrishnan TR (2006) Modelling anaerobic biofilm reactor—a review. J Environ Manag 81:1–18

Saravanan V, Sreekrishnan T (2008) A mathematical model for a hybrid anaerobic reactor. J Environ Manag 88:136–146

Satoh H, Nakamura Y, Ono H, Okabe S (2003) Effect of oxygen concentration on nitrification and denitrification in single activated sludge flocs. Biotechnol Bioeng 83:604–607

Satoh H, Onoa H, Rulinb B, Kamoc J, Okabed S, Fukushi KI (2004) Macroscale and microscale analyses of nitrification and denitrification in biofilms attached on membrane aerated biofilm reactors. Water Res 38:1633–1641

Seixo J, Varela MH, Coutinho JAP, Coelho MAZ (2004) Influence of C/N ratio on autotrophic biomass development in a sequencing batch reactor. Biochem Eng J 21:131–139

Splendiani A, Livingston AG, Nicolella C (2006) Control of membrane attached biofilms in the presence of surfactants. Biotechnol Bioeng 94:15–23

Tucker WA, Nelken LH (1982) Neural mechanisms underlying value-based decision making. In: Warren JL, William FR, David HR (eds) Handbook of chemical property estimation methods. American Chemical Society

van Haandel A, van der Lubbe J (2007) Handbook biological wastewater treatment. Quist Publishing, Leidschendam

Vieira MJ, Melo LF (1999) Intrinsic kinetics of biofilms formed under turbulent flow and low substrate concentration. Bioproc Eng 20:369–375

Viotti P, Eramo B, Boni MR, Carucci A, Leccese M, Sbaffoni S (2002) Development and calibration of a mathematical model for the simulation of the biofiltration process. Adv Environ Res 7:11–33

Walter B, Haase C, Rabiger N (2005) Combined nitrification/denitrification in a membrane reactor. Water Res 39:2781–2788

Walters E, Hillea A, Hea M, Ochmannc C, Horna H (2009) Simultaneous nitrification/denitrification in a biofilm airlift suspension (BAS) reactor with biodegradable carrier material. Water Res 43:4461–4468

Wang XM, Wang JL (2012) Denitrification of nitrate-contaminated groundwater using biodegradable snack ware as carbon source under low temperature condition. Int J Env Sci Technol 9(1):113–118

Wang Q, Zhang T (2010) Review of mathematical models for biofilms. Solid State Commun 150:1009–1022

Wang C, Li J, Wang B, Zhang G (2006) Development of an empirical model for domestic wastewater treatment by biological aerated filter. Process Biochem 41:778–782

Wanner O, Eberl H, Morgenroth E, Noguera D, Picioreanu C, Rittmann B, van Loosdrecht M, IWA Task Group on Biofilm Modeling (2006) Mathematical modeling of biofilms, Report 18. Task group members mathematical models of biofilm. Scientific and Technical IWA Publishing, London

Williamson K, Mc Carty PL (1976) A model of substrate utilization by bacterial films. J Water Pollut Con F 48:9–24